scientific reports



OPEN

The p.R321C mutation in the p62 protein is associated with abnormalities in the central nervous system

Ricardo Usategui-Martín^{1,2⊠}, Vega Esteban-López³, Estefanía Chantre-Fortes³, Manuel Sánchez-Martín^{2,4}, José A. Riancho^{5,6}, Dolores E. López^{2,3,7} & Rogelio González-Sarmiento^{1,2,8⊠}

SQSTM1/p62 has an essential role in autophagy, a catabolic pathway that is vital for maintaining cell homeostasis, p62 alterations have been observed in multiple pathological conditions, including neurodegenerative diseases and bone metabolism alterations. The p.R321C p62 protein mutation has been described in patients with amyotrophic lateral sclerosis, frontotemporal lobar degeneration, and Paget's disease of bone. In vitro studies associated the p62-321C variant with a blockade of autophagy and with the activation of the NF-kB pathway. We aimed to provide a deeper understating of the pathophysiological consequences of the p.R321C p62 mutation using a humanized mouse model. Micro-computed tomography, immunohistochemistry, and western blot analysis studied the functional consequences of the p. R321C p62 mutation. Statistical analyses were performed using SPSS software. The results showed that the p62-321C mice developed seizures after tactile-vestibular stimulation, probably associated with a blockage of the autophagy and NF-kB activation. Changes in expression of cFos and p62 were found in the amyqdala, hypothalamic nuclei, and hippocampi nuclei. In addition, numerous degenerating motor neurons were observed in the spinal cord of the p62-321C mice. We report that the blockage of the autophagy, caused by p.R321C p62 mutation, is associated with abnormalities in the central nervous system, mainly seizures after tactile-vestibular stimulation and degeneration of the motor neurons of the spinal cord but not with bone abnormalities in a humanized mouse model.

Keywords Autophagy, p62 protein, SQSTM1 gene, Neurodegeneration, Seizures

Sequestosome 1 (*SQSTM1*) gene, which encodes for p62 protein, localizes in the human chromosome 5 and comprises 8 exons distributed through 16 kb. The p62 protein has 440 amino acids (62 kDa) distributed in six functional domains, including a N-terminal Phox1 and Bem1p (PB1) domain, a zinc finger (ZZ) domain, a tumor necrosis factor receptor-associated factor 6 (TRAF6)-binding (TB) motif, an LC3-interacting region (LIR), a Keap1-interacting region (KIR), and a ubiquitin-associated (UBA) domain^{1–3}. p62 plays a crucial role in cellular signaling; it is involved in the activation of the nuclear factor kappa B (NF-kB) pathway, participates in antioxidant response by the activation of Keap1-Nrf2, and is also important in selective autophagy^{4–6}. p62 protein is expressed in both the cytoplasm and the nucleus. Flanking the TB domain are the nuclear and nuclear export signal sequences (NLS and NES) that facilitate the nuclear-to-cytoplasmic shuttling of the p62 protein⁷.

SQSTM1/p62 alterations have been observed in multiple pathological conditions^{8–10}. Missense mutations in the SQSMT1 gene have been mainly associated with bone metabolism alterations, such as Paget's disease of bone

¹Molecular Medicine Unit, Department of Medicine, Faculty of Medicine, University of Salamanca, Campus Miguel Unamuno, 37007 Salamanca, Spain. ²Institute of Biomedical Research of Salamanca (IBSAL), 37007 Salamanca, Spain. ³Institute of Neuroscience of Castilla y León (INCYL), University of Salamanca, 37007 Salamanca, Spain. ⁴Transgenic Facility, University of Salamanca, 37007 Salamanca, Spain. ⁵Department of Medicine and Psychiatry, Faculty of Medicine, University of Cantabria, IDIVAL, 39011 Santander, Spain. ⁶Internal Medicine Department, Marqués de Valdecilla University Hospital, 39008 Santander, Spain. ⁷Department of Cell Biology and Pathology, Faculty of Medicine, University of Salamanca, 37007 Salamanca, Spain. ⁸Institute of Molecular and Cellular Biology of Cancer (IBMCC), University of Salamanca-CSIC, 37007 Salamanca, Spain. [∞]email: ricardo.usategui@uva.es; gonzalez@usal.es

(PDB), and with neurodegenerative diseases like amyotrophic lateral sclerosis (ALS) or frontotemporal lobar degeneration (FTLD). One of the *SQSTM1* mutations that are common to PDB, ALS, and FTLD is the p.R321C protein variant ^{11–13}. The p.R321C mutation is near the LIR domain of the p62 protein, a domain that is crucial in autophagy due to its interaction with LC3 protein, allowing the anchoring of p62 to the autophagosome, enabling its formation and the degradation of the ubiquitinated proteins ^{14,15}. Previous functional in vitro studies conducted by our research group revealed that this mutation induces a blockage of autophagy, accumulation of the p62 protein, and activation of the NF-kB pathway¹¹. Therefore, the p.R321C variant in the p62 protein may be linked to the etiopathogenesis of PDB, ALS, and FTLD due to the role played by autophagy alterations in bone metabolism and neurodegenerative pathologies ^{16–20}. In this scenario, this study aimed to use a humanized mouse model to obtain a deeper understanding of the pathophysiological consequences of the p.R321C p62 mutation in an in vivo model.

Results

The p62-321C variant was not associated with bone alterations

The full-body CT scan did not reveal focal skeletal lesions in p62-321C mice. The microstructural analysis of the femora and tibia by μ CT did not reveal obvious abnormalities either. The results also showed no alterations in the cortical and trabecular bone of the p62-321C mice. The hematoxylin–eosin study also showed no differences in the trabecular and cortical bone of the p62-321C mice (Supplementary Fig. 1).

The p62-321C mice developed seizures and showed increased expression of cFos protein

After tactile-vestibular stimulation, the p62-321C mice developed seizures of severity 5 according to the seizure severity index²¹⁻²³. The p62-321C mice suffered generalized tonic-clonic seizures distributed bilaterally and characterized by symmetrical and bilateral spasms of the extremities, with rigidity followed by shaking. After tactile-vestibular stimulation, the animal started with an opisthotonus (arching of the cervical musculature) and then presented a generalized convulsive phase (hyperkinetic seizures with disconnection from the posterior environment) followed by a stuporous period (Supplementary Video 1). These crises occurred in all p62-321C mice, and the p62-321R mice did not develop seizures after the same stimulation.

Immunohistochemical detection of cFos-like protein was used to identify central structures activated by tactile-vestibular stimulation. The results showed that the cFos brain immunoexpression differed between p62-321C and p62-321R mice. The cFos labeling was higher in p62-321C mice than in p62-321R mice. The differences were mainly observed in the external cortex of the inferior colliculus, in the hypothalamic and amygdaloid areas, in the hippocampal formation, and in the motor cortex. In particular, cFos expression was elevated in the anterior hypothalamic and ventromedial hypothalamic areas nuclei, in the posteroventral part of the medial amygdaloid nucleus and piriform cortex of the amygdaloid nuclei, in the carnu ammonis area 3 and dentate gyrus of the hippocampal, and in the cingulate and motor cortex (Table 1 and Fig. 1).

The p62 protein expression was higher in the p62-321C mice

Western blot analysis detected higher levels of p62 and LC3B-II proteins in the brain (p=0.012 and 0.032 for p62 and LC3B-II, respectively) and spinal cord (p=0.021 and 0.028 for p62 and LC3B-II, respectively) of the p62-321C mice than in those from p62-321R mice. The expression of mTOR and beclin1 proteins were similar in p62-321C and p62-321R mice (Fig. 2). The results also revealed differences in the immunohistochemical detection of the p62 protein in the central nervous system (CNS) between the p62-321C and p62-321R mice. The density of immunopositive neurons varied across different areas of the CNS (Table 2). The main differences were in the amygdala, hypothalamic nuclei, and hippocampi nuclei, where the p62 immunoexpression was higher in p62-321C mice than in p62-321R mice (Fig. 3). In addition, the labeling was abundant and particularly strong in brainstem motor nuclei, such as the facial and trigeminal motor nucleus, the locus coeruleus, the dorsal raphe nucleus, the interpeduncular nucleus, and the pontine nuclei (Fig. 4). A more detailed distribution of the p62 immunoreactivity is shown in the Supplementary Fig. 2. In the spinal cord, the motoneurons of the p62-321C mice were more immunoreactive to p62 than those of p62-321R mice (Fig. 5A). In addition, signs of neurodegeneration were observed in the p62-321C mice. Numerous degenerating motor neurons in the spinal cord surrounded by leukocytes could be observed, particularly in areas with neurons showing the most intense staining with p62 antibodies (Fig. 5B,C).

Discussion

P62 is a multimodule adaptor protein coded by the *SQSTM1* gene that is crucial in multiple cellular processes, including NF-kB signaling, apoptosis, or Nrf2 activation²⁴. Also, the p62 protein has an essential role as a cargo receptor for ubiquitin-mediated autophagy, a crucial catabolic pathway for removing cell proteins and organelles. p62 protein interacts with ubiquitinated proteins through its UBA domain and the complex is sequestered by the autophagosome membrane by the interaction between its LIR domain and LC3 protein²⁵. Autophagy is vital for maintaining cell homeostasis, and its dysregulation is associated with various human diseases, such as cancer, metabolic disorders, and neurodegenerative diseases^{26–28}. Autophagy deficiencies have been implicated in several neurodegenerative alterations, including FTLD, ALS, Alzheimer's disease, and Huntington's disease, among others^{29–33}.

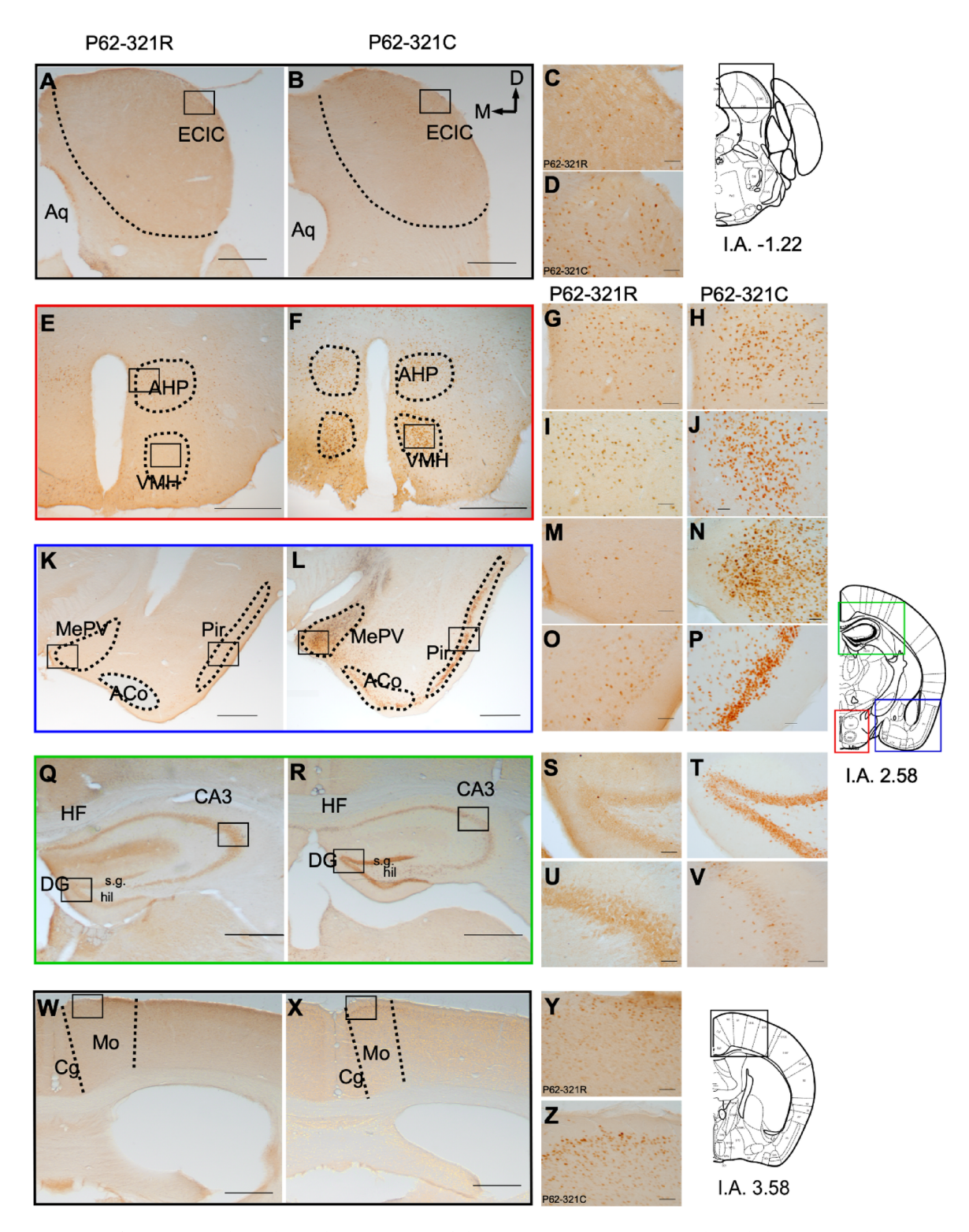
The p. R321C mutation is localized near the LIR domain of the p62 protein and has been described in patients with PDB, FTLD, and ALS^{8,11}. The LIR domain is essential in autophagy because it interacts with the LC3 protein, facilitating the anchoring of p62 to the autophagosome and enabling the degradation of ubiquitinated proteins^{14,15}. In vitro studies have shown that the 321C-p62 variant blocks autophagy and activates the NF-kB pathway. It was observed that the p.R321C mutation was associated with the formation of cytoplasmic

Main areas of the central nervous system showing c-Fos immunoreactivity	Immunopositive cell density		Labeling intensity	
			Weak	Strong
NUCLEI	p62-321R	p62-321C	p62-321R	p62-321C
Amygdaloid nuclei (anterior, medial, and cortical areas) (AA, MeA, and PCo)	+	+++		
Cingulate cortex, areas 1 and 2 (Cg1, Cg2)	+	+++		
Dorsal cortex of the inferior colliculus (DCIC)	++	+++		
Entorhinal cortex (Ent)	++	+++		
External cortex of the inferior colliculus (ECIC)	++	+++		
Hypothalamic nuclei, (anterior, posterior and Septohypothalamic area)(AHP, PH, Shy)	+	+++		
Mediodorsal thalamic nucleus (MD)	++	+++		
Piriform cortex (Pir)	++	+++		
Primary and secondary motor cortex (M1 and M2)	++	+++		
Primary and secondary somatosensory cortex (S1 and S2)	++	+++		
Primary auditory cortex (Au1)	++	+++		
Primary visual cortex, binocular área(V1b)	++	+++		
Retrosplenial granular cortex, a region (RSGa)	++	+++		
Subiculum, transition area (STr)	+	+++		
Superficial gray layer of the superior colliculus (SuG)	++	+++		
Temporal association cortex (TeA)	++	+++		
Ventrolateral periaqueductal gray (VLPAG)	+	+++		

Table 1. Immunopositive areas for the c-Fos antibody in p62-321R and p62-321C mice.

aggregates, possibly autophagosomes that could not fuse with lysosomes and, therefore, with increased levels of p62 protein 11. The levels of p62 protein can be used to monitor autophagy as it is degraded during the process; higher levels of p62 protein are linked to reduced autophagic activation 34. The p.R321C p62 protein mutation causes effects similar to those observed with chloroquine treatment, a known inductor of autophagy blockade and NF-kB activation 11,35. In this scenario, we used a humanized mouse model to determine the pathological consequences of the p.R321C mutation. Our results show that the mice carrying the p321C protein display seizures after tactile–vestibular stimulation but not bone alterations. The absence of bone abnormalities strongly suggests that a second genetic or environmental hit in the bone may be necessary in the pathophysiology of PDB.

Abnormalities in the autophagy pathway have been previously associated with neurological disorders, including epileptic seizures^{36–38}. Our results showed that p62 immunoexpression was higher in the p62-321C mice, mainly in the amygdala and in the hypothalamic nuclei. The amygdala and other limbic areas, such as the hippocampus, have been classified as trigger zones in some forms of temporal lobe epilepsy (TLE)^{39–41}. Epilepsy is one of the most common neurologic disorders in clinical practice. Epileptic seizures represent an alteration of neurologic function caused by the excessive, hypersynchronous discharge of neurons in the brain⁴⁰. The immediate early *cFos* gene has long been known as a molecular marker of neuronal activity⁴², and it has been reported that seizure activity results in increased *cFos* gene expression in particular subsets of neurons⁴³. Considering that the cFos protein is expressed in situations of neuronal activation^{42,43}, its overexpression in p62-321C mice may indicate that their neurons show higher basal activity and, therefore, an excess of electrical impulses, which are associated with a predisposition to seizures. Our experiments revealed that p62-321C mice,



after seizures, showed mainly an increase of the cFos protein expression in hypothalamic, amygdaloid, and hippocampal nuclei. These areas are considered seizure triggers in some forms of epilepsy^{39–41}. The pathways involved in seizures originating from the brainstem, such as audiogenic seizures, are well-studied^{44,45}. In our case, these reflex seizures are triggered by tactile-vestibular stimuli, and the pathways are not clearly defined. It is known that limbic seizures mainly focus on the amygdala⁴⁶, and seizures originating in the amygdala and hippocampus have also been described⁴⁷. In our case, nuclei that were intensely stained with cFos, associated with epilepsy, such as the amygdala, hippocampus, and piriform cortex⁴⁸, suggest that these nuclei may play a role in the potential pathway for this type of seizure. In many cases, seizures are aggravated in situations of stress or anxiety⁴⁹. This stress response is mediated by the hypothalamic-pituitary-adrenal axis, which would explain why p62-321C mice have a higher density of cFos protein in these areas after stimulation.

Previously, we demonstrated how the p62 p.R321C mutation induces an autophagy blockade and activates the transcriptional regulator NF-kB pathway by accumulating the p62 protein¹¹. NF-kB plays a key role in

∢Fig. 1. Distribution of the cFos protein in several nuclei of the brainstem in p62-321R and p62-321C mice after the tactile-vestibular stimulation. Scheme showing coronal sections of the brain at different rostrocaudal levels (references in relation to the interaural (I.A.) level). The images on the left show the interaural level from which the sections were prepared outlined with a box. (A,B) Fos immunoreactivity in the external cortex of the inferior colliculus. (C,D) High magnification of the square outlined in (A) and (B), respectively. (E,F) Fos immunoreactivity in the hypothalamic nuclei. (G,H) High magnification of the square outlined in the AHP in (E) and (F), respectively. (I,J) High magnification of the square outlined in the VMH in (E) and (F), respectively. (K,L) Fos immunoreactivity in the amygdaloid nuclei. (M,N) High magnification of the square outlined in the MePV in (K) and (L) respectively. (O,P) High magnification of the square outlined in the Pir in (K) and (L), respectively. (Q,R) Fos immunoreactivity in the hippocampal formation; (S,T) High magnification of the square outlined in the DG of the hippocampus in (K) and (L), respectively. (U,V) Fos immunoreactivity in the field CA3 of the hippocampus; (W,X) Fos immunoreactivity in the motor cortex; (Y,Z) High magnification of the square outlined in the Mo in (W) and (X) respectively. ACo anterior cortical amygdaloid area, Aq aqueduct, APH anterior hypothalamic nucleus, CA3 Cornu Ammonis area 3, Cg cingulate cortex, DG dentate gyrus, ECIC external cortex of the inferior colliculus, HF hippocampal formation, hil hilus, MePV medial amygdaloid nucleus, posteroventral part, Mo motor cortex, Pir piriform cortex, s.g. stratum granulosum, VMH ventromedial hypothalamic nucleus. Scale bars: 500 µm (A,B,E,F,K,L,Q,R,W and X) and 20 μm (C,D,G-J,M-P,S-V,Y and Z).

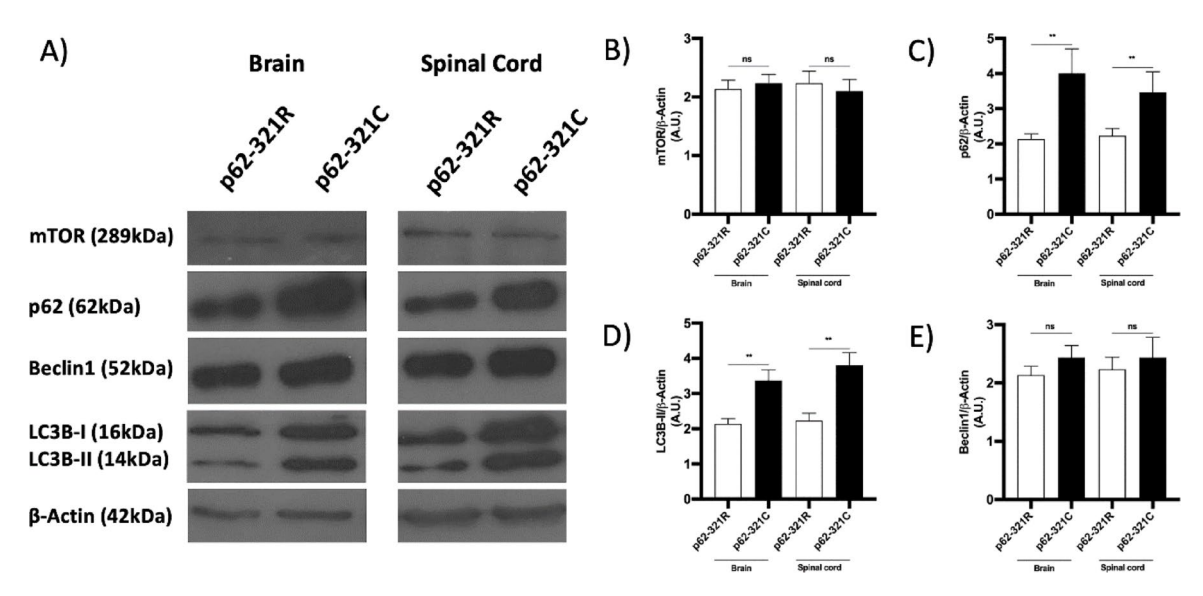


Fig. 2. Comparison of the expression of autophagy-related proteins in the brain and spinal cord in p62-321R and p62-321C mice. (**A**) mTOR, p62, LC3B and beclin1 proteins were analysed by Western blotting. (**B**–**E**) Relative protein abundance of mTOR (**B**), p62 (**C**), LC3B (**D**) and beclin1 (**E**) were quantified. All blots were derived from different parts of the same gel and were processed in parallel. Data represent the average (standard deviation) of the optical density. N = 3/per group. **p<0.01, A. U arbitrary units and N.S. not significant.

cellular activity by binding to promoter regions in the nucleus and transcribing numerous protein-coding genes, including those that support neurogenesis, neuronal death survival, and synaptic plasticity^{50–52}. In this scenario, several studies have implicated the critical role of NF-kB in epilepsy⁵³. Elevated NF-kB expression has been noted in brain tissue from animal models and patients with epilepsy, being linked to an imbalance of glutamate and gamma-aminobutyric acid, changes in ion concentrations, and modifications of synaptic functions and neuronal excitability^{54,55}. In addition, autophagic mechanisms regulate synaptic transmission and plasticity^{56,57}, and impaired autophagy could facilitate aberrant synaptic reorganization, such as mossy fiber sprouting and the formation of epileptic circuits^{58,59}. Autophagy is linked to epilepsy through observations of impaired autophagy in mouse models of epilepsy, such as those with mutations in the mTOR pathway or in the *Atg7* gene, which are essential for its activation⁶⁰. This suggests that defective autophagy may contribute to the development of epilepsy. The specific cellular and molecular mechanisms by which impaired autophagy leads to epilepsy still need to be investigated in more detail. However, it is well-known that disruption of GABA receptor function and the excitatory/inhibitory balance in the brain is a well-established mechanism contributing to epilepsy associated with autophagy modifications^{61,62}. Thus, our results support the idea that the p.R321C mutation in p62 protein is linked to epilepsy in two ways: through activating the NF-kB pathway and inhibiting autophagy.

We have also observed an accumulation of p62 protein in the spinal cord, together with numerous phagocytic cells and degenerating motor neurons, in p62-321C mice. This observation aligns with the previously reported connection between autophagy alterations and neurodegenerative disorders such as ALS²⁹. The blockade

Main areas of the central nervous system showing p62 immunoreactivity	Immunopositive cell density		Labeling intensity	
			Weak	Strong
NUCLEI	p62-321R	p62-321C	p62-321R	p62-321C
Amygdala (medial and cortical nuclei)	+	+++		
Anterior hypothalamic nucleus (AHP)	++	+++		
Dorsal raphe nucleus (DR)	+	+++		
Facial motor nucleus (7N)	++	++		
Hipocampi nuclei	++	++		
Medial Tuberal nucleus (MTu)	++	+++		
Nucleus prepositus (Pr)	++	+++		
Piriform cortex (Pir)	++	+++		
Pontine nuclei (Pn)	++	+++		
Red nucleus (R)	+	++		
Substantia nigra (SN)	+	++		
Trigeminal motor nucleus (5N)	++	++		
Ventromedial nucleus of the hypothalamus (VMH)	+	++		

Table 2. Immunopositive areas for the anti-p62 antibody in p62-321R and p62-321C mice.

of autophagy caused by the 321C variant may be linked to the neurodegeneration of spinal motor neurons, consistent with reports connecting the p. R321C p62 mutation to ALS^{8,12}.

In summary, our results strongly suggest that the p. R321C p62 mutation is insufficient to produce bone alterations associated with Paget's disease. This reinforces the hypothesis that either mutations in other genes or environmental factors are involved in this disease. Nevertheless, our observations of the CNS of the p. 321C mice suggest that this mutation could be mainly related to abnormalities in limbic areas such as the amygdala and hippocampus and increased susceptibility to seizures.

Methods

Generation of humanized p62-321C and p62-321R mice

The human *SQSTM1* cDNA was cloned into the EcoRI site of the pCAG.GS vector to generate the pCAG.GS-cSQSTM1-321R construct. The p.R321C mutation was introduced into this construct using the QuikChange site-directed mutagenesis kit (Stratagene) using primers designed to introduce a C>T base change at position +961. Primer sequences for the site-directed mutagenesis were as follows: sense 5′GAG-TCC-GAG-GGG-TGC-CCT-GAG-GAA-C-3′ and antisense 5′G-TTC-CTC-AGG-GCA-CCC-CTC-GGA-CTC-3′. Vectors were transformed into *E. coli* DH5α and plasmid DNA were purified using the Rapid DNA plasmid miniprep kit (Genedan). All constructs were verified by automated sequencing.

The CAGpro-cSQSTM1.321R-beta.globin.pA and CAGpro-cSQSTM1.321C-beta.globin.pA transgenes were isolated and purified after digestion with the restriction enzymes SalI and PscI (Thermo Scientific). Both transgenes were diluted to 5 $ng/\mu l$ in a Tris–HCl (10 mM) EDTA (0.25 mM) microinjection buffer. Recombinant DNA was microinjected into the pronucleus of one-cell-stage embryos, hybrids of the C57BL/6J and CBA/J strains, at the Transgenic Facility of the University of Salamanca. All founders were identified by polymerase chain reaction (PCR) amplification and automated sequencing using specific primers: sense 5'TGG-TAA-TCG-TGC-GAG-AGG-3' and antisense 5'GCT-GCA-GCA-GAA-GCT-GAA-3'. Founder mice were crossed with wild-type C57BL6/J mice to test germ-line transmission and establish mouse colonies. Two different transgenic mouse lines were established, one wild type and one mutated, named p62-321R and p62-321C, respectively. All mice used were C57BL6/J and were obtained from the Transgenic Service of the University of Salamanca.

All animals were housed in a temperature-controlled facility with individually ventilated cages, a standard diet, and a 12-h light—dark cycle following European Union regulations. All procedures received approval from the Ethical Committee for Animal Experimentation of the University of Salamanca and were performed following EU Directive 2010/63/EU. All methods were carried out in compliance with the relevant guidelines and regulations.

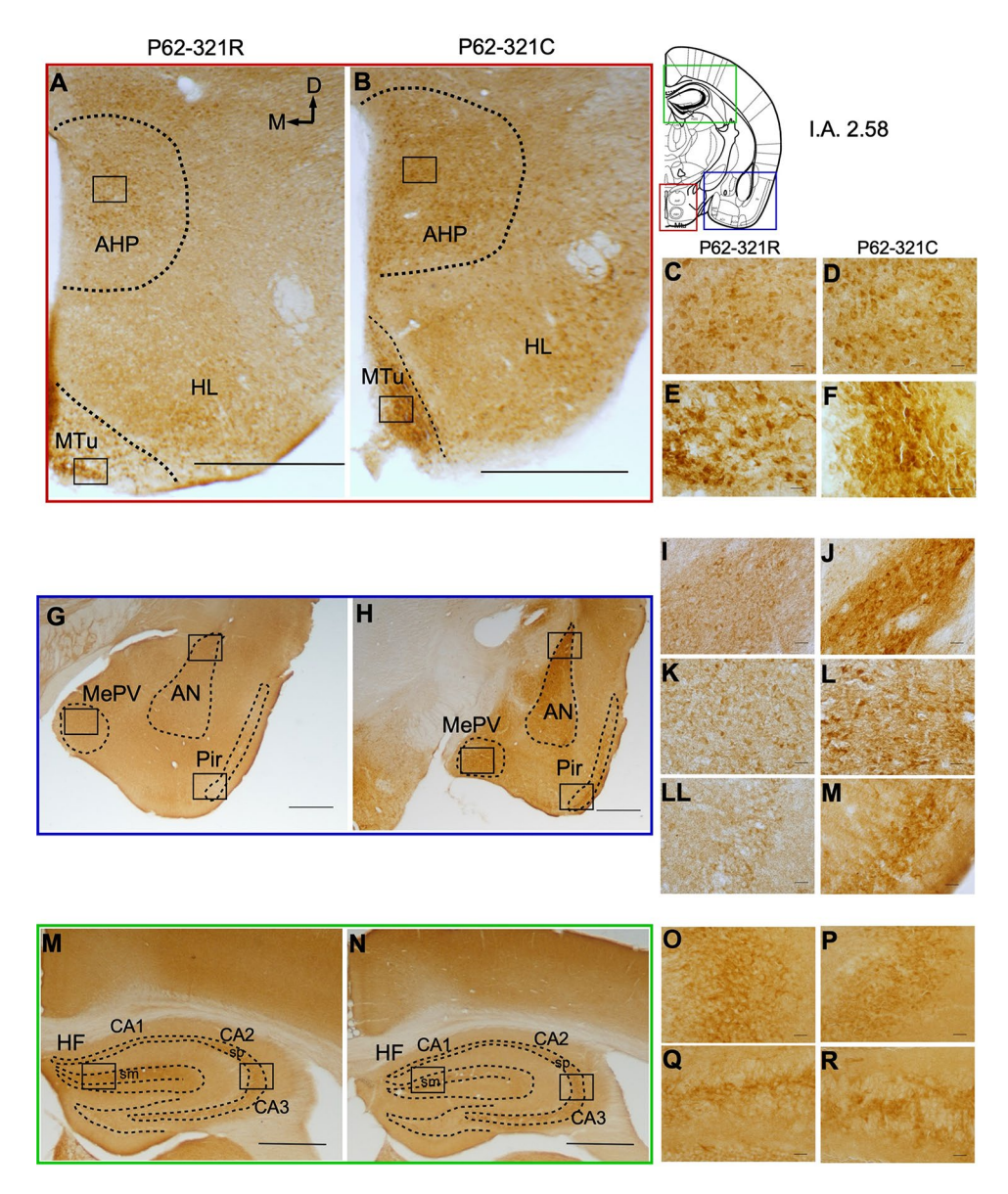


Fig. 3. Distribution of the p62 protein in the amygdala, hypothalamus and hippocampi nuclei in p62-321R and p62-321C mice. Scheme showing coronal section of the brain in relation to the interaural (I.A.) level) in p62-321R and p62-321C mice. (A,B) Hypotalamic areas. (C,D) High magnification of the square outlined in the AHP in (A) and (B), respectively. (E,F) High magnification of the square outlined in the Mtu in (A) and (B), respectively. (G,H) Amygdaloid area. (I,H) High magnification of the square outlined in the AN in (G) and (H), respectively. (K,L) High magnification of the square outlined in the MEPV in (G) and (H), respectively. (LL-M) High magnification of the square outlined in the PIR in (G) and (H), respectively. (M,N) Hippocampal formation. (O,P) High magnification of the square outlined in the s.m. in (M) and (N), respectively. (Q-R) High magnification of the square outlined in the CA3 in (M) and (N), respectively. AHP anterior hypothalamic nucleus, AN amygdaloid nuclei, CA1-3 Cornu Ammonis area 1-3, HF hippocampal formation, HL lateral hypothalamus, MePV medial amygdaloid nucleus, posteroventral part, Mtu medial tuberal nucleus, Pir piriform cortex, sm stratum moleculare, sp stratum pyramidale. Scale bars: 500 μm (A,B,G,H and N) and 20 μm (C-F,I,H,K,L,LL,M,O,P-R).

Additionally, this study adhered to the ARRIVE guidelines to ensure transparency and reproducibility. Every effort was made to minimize suffering and to utilize humane endpoints. Mice were anesthetized with 100 mg/kg ketamine and 8 mg/kg xylazine and were euthanized using carbon dioxide ($\rm CO_2$) inhalation. The sample size for each analysis included three animals per transgenic line. Male mice aged 4–6 months were used for CNS studies, while mice aged 10–12 months were utilized for analyses of bone structure. All studies described below were conducted blindly.

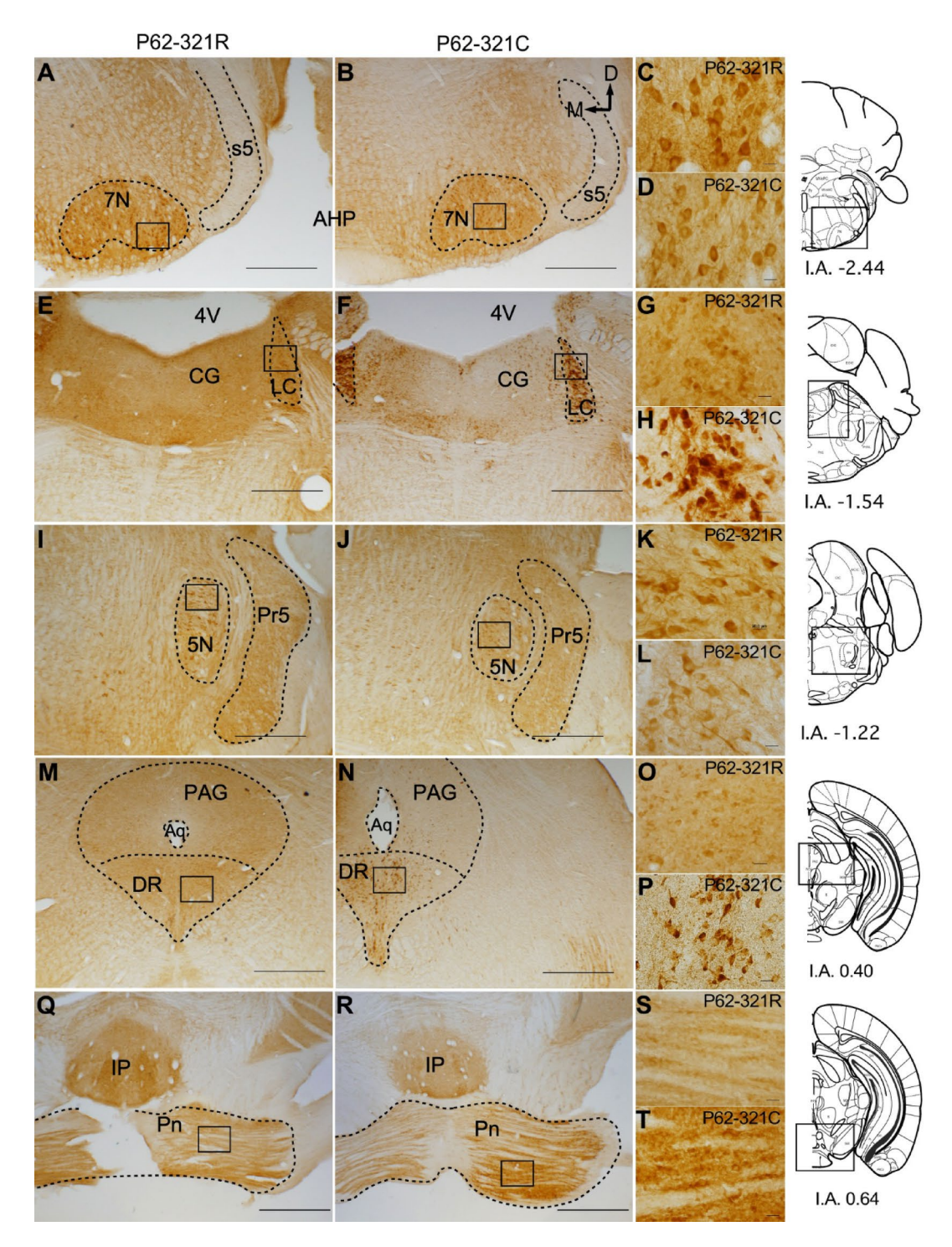


Fig. 4. Distribution of the p62 protein in several nuclei of the brainstem in p62-321R and p62-321C mice. Scheme showing coronal sections of the brain at different rostrocaudal levels in p62-321R and p62-321C mice (references in relation to the interaural (I.A.) level). The images on the left show the interaural level from which the sections were prepared outlined with a box. (A,B) P62 immunoreactivity in the facial motor nucleus. (C,D) High magnification of the square outlined in the 7N in (A) and (B), respectively. (E,F) P62 immunoreactivity in the locus coeruleus. (G,H) High magnification of the square outlined in the LC in (E) and (F), respectively. (I,J) P62 immunoreactivity in the trigeminal motor nucleus. (K,L) High magnification of the square outlined in the 5N in (I) and (J), respectively. (M,N) P62 immunoreactivity in the dorsal raphe nucleus. (O,P) High magnification of the square outlined in the DR in (M) and (N), respectively. (Q,R) P62 immunoreactivity in the interpeduncular and pontine nuclei. (S,T) High magnification of the square outlined in the Pn in (Q) and (R), respectively. Aq aqueduct, CG central gray, DR dorsal raphe nucleus, IP interpeduncular nucleus, LC locus coeruleus, PAG periaqueductal grey, Pn pontine nuclei, Pr5 principal sensory trigeminal nucleus, s5 sensory root of the trigeminal nerve, 4V 4th ventricle, 5N Trigeminal motor nucleus, 7N Facial motor nucleus. Scale bars: 500 μm (A,B,E,F,I,J,M,N,Q and R) and 20 μm (C,D,G,H,K,L,O,P,S and T).

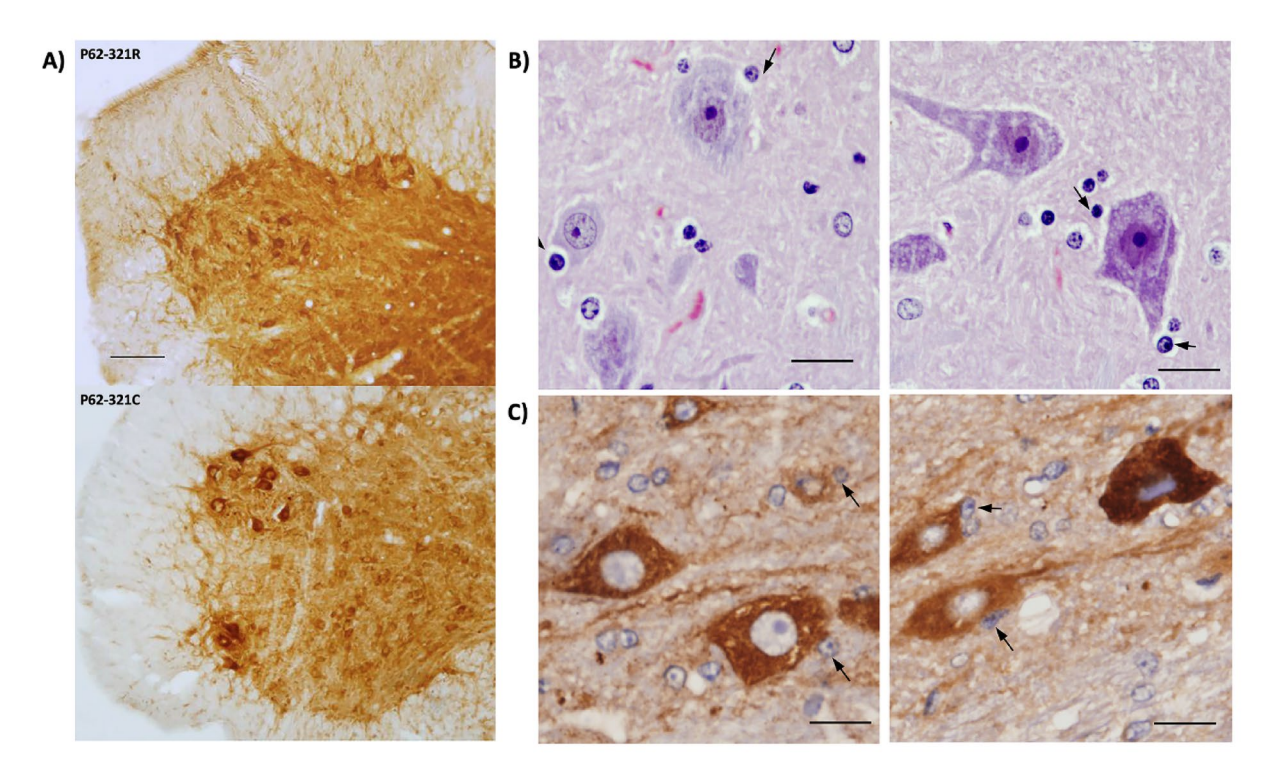


Fig. 5. Spinal motor neurons and distribution of the p62 protein in the spinal cord. (A) Coronal section of the spinal cord labeled with anti-p62 antibody in p62-321R and p62-321C mice. Scale bar: 100 μ m. The images show numerous degenerating motor neurons in the spinal cord surrounded by leukocyte (B,C). (B) Spinal cord sections were stained with Nissl and (C) labeled with anti-p62 protein antibody and counterstained with Nissl. Scale bars: 20 μ m.

Micro-computed tomography (µCT)

Whole mice were scanned, looking for focal bone lesions that could resemble PDB. Scans were obtained using a high-energy micro-computed tomography system (SkyScan 1172, Bruker Micro-CT, Kontich, Belgium) and Skyscan1172 μ CT data acquisition software (version 1.5.4.6, Bruker). Scanning was made at 50 kV and an Al 0.5 mm filter was used to reduce noise during scanning. Then, the femora and tibia were scanned at the highest resolution, with a pixel size of 6.7 μ m and voxel size of 300.8 μ m³. During the reconstruction, parameters were used to correct possible beam hardening, ring artifacts, and misalignment problems. Cortical and trabecular areas of the tibia and femur were analyzed. The structural parameters of cortical bone analyzed were tissue mineral density (TMD) and thickness. In trabecular bone, bone volume over total volume (BV/TV), bone mineral density (BMD), trabecular number (Tb.N), trabecular thickness (Tb. Th), and trabecular separation (Tb.Sp) were analyzed. The μ CT experiments were conducted on six mice (three for each genotype).

Animal stimulation

Mice received tactile–vestibular stimulation to induce seizures, which were assessed using the categorized seizure severity index (Supplementary Table 1) $^{21-23}$.

Tissue collection and processing

Bone tissue was fixed with 4% paraformaldehyde (Panreac Quimica) in phosphate-buffered saline (PBS) for 24 h at 4 °C, and it was decalcified with 5% nitric acid in PBS for 3 h. The samples were embedded in paraffin (Paraplast Plus, Leica Biosystems) using an automatic tissue processor (ASP300, Leica Microsystems), and 4- μ m sections were obtained with a rotatory microtome (Leica Microsystems). Paraffin-embedded sections were deparaffinized in xylene (Sigma-Aldrich) and rehydrated in decreasing ethanol concentrations. The sections were then stained with hematoxylin–eosin (Sigma-Aldrich). For the histological analysis of the nervous tissue, the animals were perfused through the heart with 4% paraformaldehyde in 0.1 M PBS. After perfusion, the brain and spinal cord were removed and cryoprotected by immersion in 30% sucrose for 48 h. The spinal cord was cut into 1cm sections and arranged in parallel on an agarose gel (2% in 0.1 M PB) until solidifying. The agarose gel with the spinal cord sections was placed on the holder of the vibratome, with the most rostral parts upwards and ensuring that the tissue was parallel to the cutting plane. The gel was kept cold with PB ice. Using a vibratome (Leica Microsystems), 60 μ m thickness coronal sections were cut and placed in 5 wells containing 0.1 M PB to have a representative sample of all spinal cord sections in each well. The brain was rostrocaudally pierced with a hypodermic needle to determine the laterality of the sections. Brain coronal sections were cut with a freezing sliding microtome (Leica Microsystems) at 40 μ m thickness, and serial sections were divided into a series of 6

and placed in wells containing 0.1 M PB. Each well has a representative sample of the whole brain. Additionally, the brain and spinal cord were embedded in paraffin to prepare 2- μ m coronal sections for Nissl staining (Sigma-Aldrich), which labels pyknotic nuclei and enables us to study the cytoarchitecture and subsequently select nuclei for analysis. Hematoxylin–eosin staining (Sigma-Aldrich) was also carried out. The histological analysis was performed on ten mice (five per genotype).

Determination of immunochemical markers

Free-floating sections underwent an immunohistochemistry protocol to visualize the distribution of the p62 and cFos proteins in the brain and spinal cord. After incubation with primary antibodies [anti-p62 (Abcam) and anti-cFos (Santa Cruz Biotechnology)], the sections were thoroughly rinsed and reacted for 90 min with a secondary antibody [Biotinylated goat anti-rabbit (Vector Laboratories)], following the protocols routinely used in our laboratory⁶³. As a control for the antibody labeling reaction, a set of parallel tests was performed: immunohistochemistry without the primary and secondary antibodies to identify non-specific ABC binding, immunohistochemistry without the primary and secondary antibodies as well as without the ABC to detect possible endogenous peroxidase activity, and incubation with H202 to detect potential endogenous chromogens. To analyze the results, we prepared rostrocaudally ordered coronal slices reflecting different interaural levels and used the mouse Brain in Stereotaxic Coordinates by Franklin and Paxinos⁶⁴. Immunohistochemistry was conducted to visualize the distribution of cFos protein on brain tissue from mice perfused 90 min after tactile-vestibular stimulation. The immunohistochemical detection of cFos and p62 proteins was conducted in twenty mice: ten per marker and five for each genotype.

Histological material observation

After completing the histological and immunohistochemistry protocols, all sections were mounted onto slides ordered rostrocaudally. All sections were dehydrated and coverslipped with Entellan-Neu (Merck). Sections were observed under a Leica LB30T microscope and a digital camera (Olympus DT70). All microscope parameters and settings for digitizing the photomicrographs remained constant across both experimental groups and for each animal. Pictures were taken of some sections using the software DP Controller vs 1.2.1.108. Low-magnification images were taken with the $4\times$ or $10\times$ objective lens, and high-magnification images were taken with a $40\times$ or $100\times$ objective lens (oil immersion). Morphometric measurements of labeled structures were achieved by analyzing high-magnification images with the ImageJ software (version 1.53c) as described previously 65. For the immunohistochemistry quantification, the $40\times$ objective was used, photographs were taken, and the cFos and p62-positive cells were quantified in the p62-321R mice (wild-type), and grouped into three categories: strong (+++), medium (++), and weak (+). Then, the quantification was performed in the p62-321C mice. The images were processed using Photoshop CS2 to adjust the contrast, and the figures were prepared using Canvas 14.

Western blot analysis

Brain and spinal cord tissue from p62-321R and p62-321C mice were lysed with polytron tissue homogenizer in RIPA buffer (2% sodium dodecyl sulphate, 2 mM EDTA, 2 mM EGTA, and 50 mM Tris, pH 7.5), supplemented with phosphatase inhibitors (1 mM Na $_3$ VO $_4$ and 50 mM NaF) and protease inhibitors (100 μ M phenylmethylsulfonyl fluoride, 50 μ g/ml antipapain, 50 μ g/ml pepstatin, 50 μ g/ml amastatin, 50 μ g/ml leupeptin, 50 μ g/ml bestatin, and 50 μ g/ml soybean trypsin inhibitor). Protein concentrations were determined by the BCA (bicinchoninic acid) method, using bovine serum albumin as a standard (BCA Protein Assay kit; Thermo Fisher Scientific). Protein extracts were boiled for 5 min and fractionated by SDS-PAGE, transferred to an Immobilon-P membrane (Millipore), and incubated with primary specific antibodies anti-p62 (Abcam), anti-LC3B (Novus Biologicals), anti-mTOR (Cell Signaling), anti-beclin1 (Abcam), and anti- β -actin (Thermo Fisher). The ECL Plus Detection System (GE-Healthcare) with HRP conjugated anti-mouse (for anti- β -actin) (Thermo Fisher) or anti-rabbit (for anti-p62, anti-LC3B, anti-mTOR, and anti-beclin1) (Thermo Fisher) secondary antibodies were used for detection. The protein analysis experiments were conducted in ten mice (five per genotype).

Statistical analysis

Statistical analyses were performed using the SPSS version 22.0 statistical package (SPSS). When the data were normally distributed, we applied an analysis of variance (ANOVA), whereas if data were not normally distributed, we used the Kruskal–Wallis test. Differences with a p value < 0.05 were considered statistically significant.

Data availability

All data generated during and/or analyzed during the current study are available from the corresponding author upon reasonable request.

Received: 18 November 2024; Accepted: 30 April 2025

Published online: 15 May 2025

References

- Lamark, T., Svenning, S. & Johansen, T. Regulation of selective autophagy: The p62/SQSTM1 paradigm. Essays Biochem. 61, 609–624 (2017).
- 2. Sánchez-Martín, P. & Komatsu, M. p62/SQSTM1—Steering the cell through health and disease. J. Cell Sci. 131, jcs222836 (2018).
- 3. Seibenhener, M. L., Geetha, T. & Wooten, M. W. Sequestosome 1/p62-more than just a scaffold. FEBS Lett. 581, 175-179 (2007).
- Sanz, L., Diaz-Meco, M. T., Nakano, H. & Moscat, J. The atypical PKC-interacting protein p62 channels NF-κB activation by the IL-1-TRAF6 pathway. EMBO J. 19, 1576–1586 (2000).

- 5. Komatsu, M. et al. The selective autophagy substrate p62 activates the stress responsive transcription factor Nrf2 through inactivation of Keap1. Nat. Cell Biol. 12, 213-223 (2010).
- 6. Rogov, V., Dötsch, V., Johansen, T. & Kirkin, V. Interactions between autophagy receptors and ubiquitin-like proteins form the molecular basis for selective autophagy. *Mol. Cell* **53**, 167–178 (2014).
- 7. Pankiv, S. et al. Nucleocytoplasmic shuttling of p62/SQSTM1 and its role in recruitment of nuclear polyubiquitinated proteins to promyelocytic leukemia bodies. *J. Biol. Chem.* **285**, 5941–5953 (2010).
- 8. Rea, S. L., Majcher, V., Searle, M. S. & Layfield, R. SQSTM1 mutations—Bridging Paget disease of bone and ALS/FTLD. Exp. Cell Res. 325, 27–37 (2014).
- 9. Li, L. et al. SQSTM1 is a pathogenic target of 5q copy number gains in kidney cancer. Cancer Cell 24, 738-750 (2013).
- 10. Zatloukal, K. et al. From Mallory to Mallory-Denk bodies: What, how and why?. Exp. Cell Res. 313, 2033-2049 (2007)
- 11. Usategui-Martín, R. et al. A mutation in p62 protein (p. R321C), associated to Paget's disease of bone, causes a blockade of autophagy and an activation of NF-kB pathway. Bone 133, 115265 (2020).
- 12. Fecto, F. et al. SQSTM1 mutations in familial and sporadic amyotrophic lateral sclerosis. Arch. Neurol. 68, 1440-1446 (2011).
- 13. van der Zee, J. et al. Rare mutations in SQSTM1 modify susceptibility to frontotemporal lobar degeneration. *Acta Neuropathol.* **128**, 397–410 (2014).
- Geng, J. & Klionsky, D. J. The Atg8 and Atg12 ubiquitin-like conjugation systems in macroautophagy. EMBO Rep. 9, 859–864 (2008).
- 15. Pankiv, S. et al. p62/SQSTM1 binds directly to Atg8/LC3 to facilitate degradation of ubiquitinated protein aggregates by autophagy*. *J. Biol. Chem.* 282, 24131–24145 (2007).
- Usategui-Martín, R. et al. Polymorphisms in autophagy genes are associated with paget disease of bone. PLoS ONE 10, e0128984 (2015).
- 17. Zatloukal, K. et al. p62 Is a common component of cytoplasmic inclusions in protein aggregation diseases. Am. J. Pathol. 160, 255–263 (2002).
- 18. Ralston, S. H. & Layfield, R. Pathogenesis of Paget disease of bone. Calcif. Tissue Int. 91, 97-113 (2012).
- 19. Daroszewska, A. et al. A point mutation in the ubiquitin-associated domain of SQSMT1 is sufficient to cause a Paget's disease-like disorder in mice. *Hum. Mol. Genet.* 20, 2734–2744 (2011).
- 20. Nixon, R. A. The role of autophagy in neurodegenerative disease. Nat. Med. 19, 983-997 (2013).
- 21. Doretto, M. C., Cortes-de-Oliveira, J. A., Rossetti, F. & Garcia-Cairasco, N. Role of the superior colliculus in the expression of acute and kindled audiogenic seizures in Wistar audiogenic rats. *Epilepsia* 50, 2563–2574 (2009).
- 22. Garcia-Cairasco, N. et al. Neuroethological and morphological (Neo-Timm staining) correlates of limbic recruitment during the development of audiogenic kindling in seizure susceptible Wistar rats. *Epilepsy Res.* 26, 177–192 (1996).
- 23. Rossetti, F., Rodrigues, M. C. A., de Oliveira, J. A. C. & Garcia-Cairasco, N. EEG wavelet analyses of the striatum-substantia nigra pars reticulate-superior colliculus circuitry: Audiogenic seizures and anticonvulsant drug administration in Wistar audiogenic rats (War strain). *Epilepsy Res.* 72, 192–208 (2006).
- 24. Moscat, J., Diaz-Meco, M. T. & Wooten, M. W. Signal integration and diversification through the p62 scaffold protein. *Trends Biochem. Sci.* 32, 95–100 (2007).
- 25. Ichimura, Y. & Komatsu, M. Selective degradation of p62 by autophagy. Semin. Immunopathol. 32, 431-436 (2010).
- 26. Lei, Y. & Klionsky, D. J. The emerging roles of autophagy in human diseases. Biomedicines 9, 1651 (2021).
- 27. Klionsky, D. J. et al. Autophagy in major human diseases. EMBO J. 40, e108863 (2021).
- 28. Mizushima, N. & Levine, B. Autophagy in human diseases. N. Engl. J. Med. 383, 1564-1576 (2020).
- 29. Menzies, F. M., Fleming, A. & Rubinsztein, D. C. Compromised autophagy and neurodegenerative diseases. *Nat. Rev. Neurosci.* 16, 345–357 (2015).
- Yao, L. et al. MicroRNA-124 regulates the expression of p62/p38 and promotes autophagy in the inflammatory pathogenesis of Parkinson's disease. FASEB J. 33, 8648–8665 (2019).
- 31. Yao, L. et al. LRRK2 Gly2019Ser mutation promotes ER stress via interacting with THBS1/TGF-β1 in Parkinson's disease. *Adv. Sci.* (*Weinh.*) **10**, e2303711 (2023).
- 32. Yao, L. et al. Translational evaluation of metabolic risk factors impacting DBS efficacy for PD-related sleep and depressive disorders: Preclinical, prospective and cohort studies. *Int. J. Surg.* 111, 543–566 (2025).
- 33. Lei, Y. & Klionsky, D. J. Transcriptional regulation of autophagy and its implications in human disease. *Cell Death Differ.* 30, 1416–1429 (2023).
- 34. Klionsky, D. J. et al. Guidelines for the use and interpretation of assays for monitoring autophagy (3rd edition). Autophagy 12, 1–222 (2016).
- 35. Yang, S., Qiang, L., Sample, A., Shah, P. & He, Y.-Y. NF-κB signaling activation induced by chloroquine requires autophagosome, p62 protein, and c-Jun N-terminal kinase (JNK) signaling and promotes tumor cell resistance. *J. Biol. Chem.* **292**, 3379–3388 (2017).
- 36. Ali, N. H. et al. Autophagy and autophagy signaling in epilepsy: Possible role of autophagy activator. Mol. Med. 29, 142 (2023).
- 37. Lv, M. & Ma, Q. Autophagy and epilepsy. Adv. Exp. Med. Biol. 1207, 163–169 (2020).
- 38. Fassio, A. et al. Emerging role of the autophagy/lysosomal degradative pathway in neurodevelopmental disorders with epilepsy. Front. Cell. Neurosci. 14, 39 (2020).
- Heinz-Gregor Wieser for the ILAE Commission on Neurosurgery of Epilepsy. Mesial temporal lobe epilepsy with hippocampal sclerosis. Epilepsia 45, 695–714 (2004).
- 40. Stafstrom, C. E. & Carmant, L. Seizures and epilepsy: An overview for neuroscientists. *Cold Spring Harb. Perspect. Med.* **5**, a022426 (2015).
- 41. Wu, Q., Zhao, C. W., Long, Z., Xiao, B. & Feng, L. Anatomy based networks and topology alteration in seizure-related cognitive outcomes. Front. Neuroanat. 12, 25 (2018).
- 42. Chung, L. A brief introduction to the transduction of neural activity into Fos signal. Dev. Reprod. 19, 61-67 (2015).
- 43. Morgan, J. I., Cohen, D. R., Hempstead, J. L. & Curran, T. Mapping patterns of c-fos expression in the central nervous system after seizure. *Science* 237, 192–197 (1987).
- 44. Millan, M. H., Meldrum, B. S., Boersma, C. A. & Faingold, C. L. Excitant amino acids and audiogenic seizures in the genetically epilepsy-prone rat. II. Efferent seizure propagating pathway. *Exp. Neurol.* **99**, 687–698 (1988).
- 45. Garcia-Cairasco, N., Terra, V. C. & Doretto, M. C. Midbrain substrates of audiogenic seizures in rats. *Behav. Brain Res.* **58**, 57–67 (1993).
- Dutra Moraes, M. F., Galvis-Alonso, O. Y. & Garcia-Cairasco, N. Audiogenic kindling in the Wistar rat: A potential model for recruitment of limbic structures. Epilepsy Res. 39, 251–259 (2000).
- 47. Padró, L. & Rovira, R. Diagnosis of seizures originating in the amygdala and the hippocampus. Rev. Neurol. 26, 261-265 (1998).
- 48. Vaughan, D. N. & Jackson, G. D. The piriform cortex and human focal epilepsy. Front. Neurol. 5, 259 (2014).
- 49. Maguire, J. & Salpekar, J. A. Stress, seizures, and hypothalamic–pituitary–adrenal axis targets for the treatment of epilepsy. *Epilepsy Behav.* 26, 352–362 (2013).
- 50. Mattson, M. P., Culmsee, C., Yu, Z. & Camandola, S. Roles of nuclear factor κB in neuronal survival and plasticity. *J. Neurochem.* 74, 443–456 (2000).
- 51. Mattson, M. P. & Meffert, M. K. Roles for NF-κB in nerve cell survival, plasticity, and disease. Cell Death Differ. 13, 852–860 (2006).
- 52. Sarnico, I. et al. NF-kappaB dimers in the regulation of neuronal survival. Int. Rev. Neurobiol. 85, 351-362 (2009).

- 53. Cai, M. & Lin, W. The function of NF-kappa B during epilepsy, a potential therapeutic target. Front. Neurosci. 16, 851394 (2022).
- 54. Lerner-Natoli, M., Montpied, P., Rousset, M. C., Bockaert, J. & Rondouin, G. Sequential expression of surface antigens and transcription factor NFkappaB by hippocampal cells in excitotoxicity and experimental epilepsy. *Epilepsy Res.* 41, 141–154 (2000).
- Lubin, F. D., Ren, Y., Xu, X. & Anderson, A. E. Nuclear factor-κB regulates seizure threshold and gene transcription following convulsant stimulation. J. Neurochem. 103, 1381–1395 (2007).
- 56. Shen, W. & Ganetzky, B. Autophagy promotes synapse development in Drosophila. J. Cell Biol. 187, 71-79 (2009).
- 57. Hernandez, D. et al. Regulation of presynaptic neurotransmission by macroautophagy. Neuron 74, 277-284 (2012).
- 58. Limanaqi, F. et al. mTOR-related cell-clearing systems in epileptic seizures, an update. *Int. J. Mol. Sci.* 21, 1642 (2020).
- 59. McMahon, J. et al. Impaired autophagy in neurons after disinhibition of mammalian target of rapamycin and its contribution to epileptogenesis. *J. Neurosci.* **32**, 15704–15714 (2012).
- 60. Wong, M. Cleaning up epilepsy and neurodegeneration: The role of autophagy in epileptogenesis. *Epilepsy Curr.* 13, 177–178 (2013)
- Kang, J.-Q., Shen, W., Lee, M., Gallagher, M. J. & Macdonald, R. L. Slow degradation and aggregation in vitro of mutant GABAA receptor γ2(Q351X) subunits associated with epilepsy. J. Neurosci. 30, 13895–13905 (2010).
- 62. Tipton, A. E. & Russek, S. J. Regulation of inhibitory signaling at the receptor and cellular level; Advances in our understanding of GABAergic neurotransmission and the mechanisms by which it is disrupted in epilepsy. *Front. Synaptic Neurosci.* 14, 914374 (2022).
- 63. Sánchez-Benito, D., Hyppolito, M. A., Alvarez-Morujo, A. J., López, D. E. & Gómez-Nieto, R. Morphological and molecular correlates of altered hearing sensitivity in the genetically audiogenic seizure-prone hamster GASH/Sal. *Hear. Res.* **392**, 107973 (2020).
- 64. Paxinos, G. & Franklin, K. B. J. The Mouse Brain in Stereotaxic Coordinates (Elsevier Science, 2007).
- 65. Gómez-Nieto, R. et al. A fast cholinergic modulation of the primary acoustic startle circuit in rats. *Brain Struct. Funct.* **219**, 1555–1573 (2014).

Acknowledgements

We thank Ms. Nieves Mateos for her technical help.

Author contributions

RUM, DEL, and RGS designed this research; RUM, VEL, ECF, MSM, JAR, DEL, and RGS performed the experiments. RUM, JAR, DEL, and RGS performed statistical analysis and data interpretation. RUM, DEL, and RGS wrote the manuscript. All authors read and approved the final manuscript. RGS is the supervisor of this work who has full access to all the data in the study and takes responsibility for the data integrity and accuracy.

Funding

This work was funded by Projects ISC IIII-FEDER: PI16/01920 and PI20/01589 from Instituto de Salud Carlos III (Ministry of Science and Innovation).

Declarations

Competing interests

The authors declare no competing interests.

Additional information

Supplementary Information The online version contains supplementary material available at https://doi.org/1 0.1038/s41598-025-00764-2.

Correspondence and requests for materials should be addressed to R.U.-M. or R.G.-S.

Reprints and permissions information is available at www.nature.com/reprints.

Publisher's note Springer Nature remains neutral with regard to jurisdictional claims in published maps and institutional affiliations.

Open Access This article is licensed under a Creative Commons Attribution-NonCommercial-NoDerivatives 4.0 International License, which permits any non-commercial use, sharing, distribution and reproduction in any medium or format, as long as you give appropriate credit to the original author(s) and the source, provide a link to the Creative Commons licence, and indicate if you modified the licensed material. You do not have permission under this licence to share adapted material derived from this article or parts of it. The images or other third party material in this article are included in the article's Creative Commons licence, unless indicated otherwise in a credit line to the material. If material is not included in the article's Creative Commons licence and your intended use is not permitted by statutory regulation or exceeds the permitted use, you will need to obtain permission directly from the copyright holder. To view a copy of this licence, visit https://creativecommons.org/licenses/by-nc-nd/4.0/.

© The Author(s) 2025